

# Dust abundance and grain size in galaxy halos

Hiroiyuki Hirashita<sup>a</sup>, Chih-Yu Lin<sup>a,b</sup>

<sup>a</sup>*Institute of Astronomy and Astrophysics, Academia Sinica, P.O. Box 23-141, Taipei 10617, Taiwan*

<sup>b</sup>*Department of Physics, National Chung Hsing University, 145 Xingda Rd., South Dist., Taichung 40227, Taiwan*

---

## Abstract

We investigate the abundance and properties (especially, grain size) of dust in galaxy halos using available observational data in the literature. There are two major sets of data. One is (i) the reddening curves at redshifts  $z \sim 1$  and 2 derived for Mg II absorbers, which are assumed to trace the medium in galaxy halos. The other is (ii) the cosmic extinction up to  $z \sim 2$  mainly traced by distant background quasars. For (i), the observed reddening curves favor a grain radius of  $a \sim 0.03 \mu\text{m}$  for silicate, while graphite is not supported because of its strong 2175 Å bump. Using amorphous carbon improves the fit to the reddening curves compared with graphite if the grain radius is  $a \lesssim 0.03 \mu\text{m}$ . For (ii), the cosmic extinction requires  $\eta \gtrsim 10^{-2}$  ( $\eta$  is the ratio of the halo dust mass to the stellar mass; the observationally suggested value is  $\eta \sim 10^{-3}$ ) for silicate if  $a \sim 0.03 \mu\text{m}$  as suggested by the reddening curve constraint. Thus, for silicate, we do not find any grain radius that satisfies both (i) and (ii) unless the halo dust abundance is much larger than suggested by the observations. For amorphous carbon, in contrast, a wide range of grain radius ( $a \sim 0.01\text{--}0.3 \mu\text{m}$ ) is accepted by the cosmic extinction; thus, we find that a grain radius range of  $a \sim 0.01\text{--}0.03 \mu\text{m}$  is supported by combining (i) and (ii). We also discuss the origin of dust in galaxy halos, focusing on the importance of grain size in the physical mechanism of dust supply to galaxy halos.

**Keywords:** Dust, Galaxies, Galaxy halos, Circum-galactic medium

---

## 1. Introduction

The interstellar dust is known to occupy around 1% of the total mass of the interstellar medium (ISM) in the Milky Way, which means that around half of the metals<sup>1</sup> are in the solid (dust) phase (e.g. Evans, 1994; Jenkins, 2009). Dust forms and evolves mainly in the ISM of galaxies through various processes (Asano et al., 2013). Since a galaxy is not a closed system, the ISM interacts with the circum-galactic medium (CGM) and the intergalactic medium (IGM) through outflow driven by supernovae (SNe) and active galactic nuclei (AGNs) (e.g., Veilleux et al., 2005), and through inflow driven by cooling and/or gravity (e.g., Kereš et al., 2005). The outflow could also transport the interstellar dust to the CGM and IGM (Zu et al., 2011; McKinnon et al., 2016; Hou et al., 2017; Aoyama et al., 2018). Radiation pressure from newly formed stars in a galaxy could also drive the interstellar dust outward, supplying the dust to the CGM and IGM (Ferrara et al., 1991; Bianchi and Ferrara, 2005; Bekki, 2015). Therefore, the cosmic dust has a wide spatial distribution not limited to the ISM but extended over the cosmological volume (see also Aguirre, 1999).

The dust content in galaxy halos (or the CGM; hereafter, we simply use words “galaxy halo” to indicate the circum-galactic environment up to a radius of  $\sim 100\text{--}200$  kpc) gives us a clue to the transport of dust from the ISM to the IGM,

since galaxy halos are the interface between the ISM and the IGM. Ménard et al. (2010, hereafter M10) detected reddening<sup>2</sup> in galaxy halos using the cross-correlation between the galaxy position and the reddening of background quasi-stellar objects (QSOs) for a large sample of galaxies taken by the Sloan Digital Sky Survey (SDSS; York and et al. 2000). The median redshift of their sample is  $z \sim 0.3$  ( $z$  denotes the redshift). They detected reddening up to a radius of several Mpc from the galaxy center. Peek et al. (2015) applied basically the same method to nearby galaxies ( $z \sim 0.05$ ), and found a similar radial profile of reddening to the one found in M10. Masaki and Yoshida (2012) confirmed the observationally suggested large extent of dust distribution in galaxy halos by comparing their analytic halo model with M10’s data.

The existence of dust in galaxy halos is important in the following aspects. Dust contained in galaxy halos on a line of sight causes dust extinction on a cosmological distance scale. This could lead to a systematic reddening effect on distant QSOs and SNe. Dust in galaxy halos is also of fundamental importance in the total dust budget in galaxies and in the Universe, since M10 estimate that the dust mass in a galaxy halo is on average comparable to that in a galaxy disc. Moreover, as Inoue and Kamaya (2003, 2004) argued, dust in the IGM could affect the thermal state of the IGM through photoelectric heating. They constrained the grain size and the dust-to-

---

*Email address:* hirashita@asiaa.sinica.edu.tw (Hiroiyuki Hirashita)

<sup>1</sup>We refer to elements heavier than helium (such as C, N, O, etc.) as metals, following the convention in astronomy.

---

<sup>2</sup>In this paper, we define the reddening as the difference between the dust extinctions (usually expressed in units of magnitude) at two wavelengths. Since dust extinction tends to be larger at shorter wavelengths, the color usually becomes redder than the intrinsic one after dust extinction.

gas ratio in the IGM using the observed thermal history of the IGM, although those two quantities are degenerate in such a way that small grains require smaller abundance of dust. It is also important to note that dust extinction strongly depends on grain size (or grain size distribution) and dust-to-gas ratio (Inoue and Kamaya, 2004, 2010). Thus, among dust grain properties, we focus on grain size and dust-to-gas ratio (or dust abundance) in this paper.

To clarify the dust properties in galaxy halos, it would be observationally convenient to target specific objects that represent the CGM. Ménard and Fukugita (2012, hereafter MF12) argued that Mg II absorbers trace the gas in galaxy halos, based on the impact parameters. The estimated dust-to-gas ratio for Mg II absorbers is also consistent with that expected for  $L^*$  galaxies, which indicates that Mg II absorbers are associated with  $\sim L^*$  galaxies (i.e., galaxies with the characteristic optical luminosity in the luminosity function) (Ménard and Chelouche, 2009). Deep imaging observations also support this association (Steidel et al., 1997; Zibetti et al., 2007). MF12 pointed out that, if Mg II absorbers are associated with outflow originating from metal-enriched galaxies, their dust-to-gas ratios comparable to the Milky Way dust-to-gas ratio ( $\sim 1/100$ ) can be naturally explained. Although we should keep in mind that the origin of Mg II absorbers has still been debated, there are some observations that showed a link between Mg II absorbers and outflows driven by stellar feedback (energy input from stars) (Bond et al., 2001; Tremonti et al., 2007; Bouché et al., 2007).

York et al. (2006) studied about 800 Mg II absorbers at  $z \approx 1.0$ – $1.9$ . By comparing sub-samples with various absorption strength, they derived the extinction curves for those absorbers, finding that they are described well by the Small Magellanic Cloud (SMC) extinction curve. MF12 analyzed the reddening of background QSOs and derived reddening curves (reddening as a function of rest-frame wavelengths) for Mg II absorbers at  $z \sim 1$  and 2. They found that the reddening curves are fitted well with the SMC extinction curve. For nearby ( $z \sim 0.05$ ) galaxies, Peek et al. (2015) derived a similar reddening curve to the one obtained above, except for the strong excess in the  $u$ -band (i.e., at the shortest among their sampled wavelengths). The strongly rising trend toward short wavelengths ( $\lambda \lesssim 0.2 \mu\text{m}$ , where  $\lambda$  is the rest-frame wavelength) in the SMC extinction curve, which is consistent with the reddening curves of Mg II absorbers, indicates the existence of grains with radii smaller than  $\lambda/(2\pi) \sim 0.03 \mu\text{m}$  (Bohren and Huffman, 1983). In other words, the reddening curves could be used to obtain the information on grain size in galaxy halos.

In this paper, we aim at putting a constraint on the dust grain size and the dust abundance in galaxy halos based on the currently available data in the literature. The obtained constraints on those quantities could be used to clarify the origin and evolution of dust in galaxy halos. Although our analysis is limited by the current uncertainty in the observational data, we make a first attempt to draw a useful conclusion about the grain size as we see later. We also discuss some theoretical predictions in the literature on the dust properties in galaxy halos, and comment on the limitation of the current knowledge on dust in galaxy halos.

The paper is organized as follows. We formulate the model of reddening curves and dust extinction in Section 2. We show the results and compare them with observational data in Section 3. We further discuss the model predictions in terms of theoretical predictions in the literature, and clarify the limitation of our knowledge on halo dust in Section 4. Finally we conclude in Section 5. Throughout this paper, we adopt  $H_0 = 70 \text{ km s}^{-1} \text{ Mpc}^{-1}$ ,  $\Omega_M = 0.3$ , and  $\Omega_\Lambda = 0.7$  for the cosmological parameters.

## 2. Model

We construct a model that describes the reddening caused by dust in galaxy halos. We mainly treat the wavelength dependence of reddening, which we refer to as the *reddening curve*, and the extinction over the cosmic distance, which we refer to as the *cosmic extinction*. We formulate those quantities in what follows.

### 2.1. Reddening

The wavelength dependence of extinction can be used to constrain dust properties, especially grain size. Although it is difficult to measure the extinction in a single band, the color excess or reddening, which is a relative flux change at two wavelengths due to dust extinction, is rather easily derived. The reddening is defined as the difference in the extinctions at  $\lambda_1$  and  $\lambda_2$  ( $\lambda_1 > \lambda_2$ ).

The currently available data for dust in galaxy halos are not precise enough to constrain the detailed grain size distribution. The functional form of the grain size distribution and the maximum and minimum of grain radius are degenerate (i.e., it is usually difficult to determine all those properties uniquely), especially when the reddening is given with a sparse sampling of wavelengths. Thus, we assume that all the dust grains have a single radius,  $a$ , for simplicity. This simple assumption is useful to obtain the typical radius of dust grains that dominate the opacity in galaxy halos. We additionally discuss the effect of grain size distribution in Section 4.2.

To evaluate the extinction, we need the mass extinction coefficient (the cross-section for extinction per dust mass),  $\kappa_{\text{ext}}(\lambda)$  (Hildebrand, 1983):

$$\kappa_{\text{ext}}(\lambda) = \frac{3Q_{\text{ext}}(\lambda, a)}{4as}, \quad (1)$$

where  $Q_{\text{ext}}(\lambda, a)$  is the extinction cross-section per geometric cross-section, and the grains are assumed to be spherical with grain radius  $a$  and material density  $s$ . We calculate  $Q_{\text{ext}}$  using the Mie theory with grain properties in the literature (Section 2.3). The extinction at wavelength  $\lambda$ ,  $A_\lambda$ , is estimated as

$$A_\lambda = 2.5(\log e) \kappa_{\text{ext}}(\lambda) \mu m_{\text{H}} N_{\text{H}} \mathcal{D}, \quad (2)$$

where  $\mu (= 1.4)$  is the gas mass per hydrogen,  $m_{\text{H}}$  is the mass of hydrogen atom,  $N_{\text{H}}$  is the column density of hydrogen nuclei, and  $\mathcal{D}$  is the dust-to-gas ratio.

Since the reddening  $A_{\lambda_1} - A_{\lambda_2}$  is proportional to  $N_{\text{H}}\mathcal{D}$ ,<sup>3</sup> we need to adopt objects whose column density and dust-to-gas ratio are well constrained. Following MF12, we use Mg II absorbers as tracers of dust in galaxy halos (see the Introduction). According to MF12, the typical column density of an Mg II absorber is  $N_{\text{H}} \sim 10^{19.5} \text{ cm}^{-2}$ , and the dust-to-gas ratio is 60–80 per cent of the Milky Way value if we use  $A_V/N_{\text{H}}$  for the indicator of dust-to-gas ratio. Assuming the typical dust-to-gas ratio of the Milky Way to be 0.01 (or slightly less) (e.g., Pei, 1992), we adopt  $\mathcal{D} \sim 0.006$  for Mg II absorbers. Peek et al. (2015) derived a reddening curve for galaxy halos at  $z \sim 0.05$ . Their reddening curve is similar to the one obtained by MF12, except for the strong excess of extinction in the  $u$ -band (i.e., at the shortest wavelength among their bands). As we see later, the column density, which is poorly known for galaxy halos, is also important. Because of the well estimated column density for Mg II absorbers, we adopt the data in MF12.

## 2.2. Extinction over the cosmic distance (cosmic extinction)

Dust enrichment in galactic halos has not been fully understood yet. Thus, as a starting point, we simply scale the halo dust mass with the stellar mass in the galaxy. This may be a reasonable starting point because the dust is most probably supplied to the halo as a result of stellar feedback (MF12; Hou et al. 2017). Masaki and Yoshida (2012) also adopted this assumption in their model that reproduced a consistent dust distribution to M10’s observation data. From that assumption, the dust mass in the halo,  $M_{\text{d,halo}}$  can be expressed as

$$M_{\text{d,halo}} = \eta M_{\text{star}}, \quad (3)$$

where  $M_{\text{star}}$  is the stellar mass and  $\eta$  is the mass ratio of the dust in the halo to stars. Peek et al. (2015) showed, using a sample at  $z \sim 0.05$ , that  $M_{\text{d,halo}} \propto M_{\text{star}}^{0.23}$ . Thus, in general,  $\eta$  depends on  $M_{\text{star}}$ .

The statistics of the stellar mass per comoving volume in the Universe is described by the stellar mass function (probability distribution function of galaxies with stellar mass  $M_{\text{star}}$ ),  $\Phi(M_{\text{star}})$ . We adopt the stellar mass function at  $z < 3$  from Tomczak et al. (2014). We estimate the comoving halo dust density,  $\rho_{\text{d,halo}}$ , as

$$\begin{aligned} \rho_{\text{d,halo}} &= \int M_{\text{d,halo}} \Phi(M_{\text{star}}) dM_{\text{star}}, \\ &= \langle \eta \rangle \rho_{\text{star}}, \end{aligned} \quad (4)$$

where the integration range for the stellar mass is the same ( $10^9 M_{\odot} < M_{\text{star}} < 10^{13} M_{\odot}$ ) as in Tomczak et al. (2014),  $\langle \eta \rangle$  is the average of  $\eta$  for the corresponding stellar mass range, and  $\rho_{\text{star}}$  is the comoving stellar mass density (Appendix A). We adopt the following fitting for  $\rho_{\text{star}}$  as a function of redshift  $z$  as (Tomczak et al., 2014)

$$\log \rho_{\text{star}} [M_{\odot} \text{ Mpc}^{-3}] = -0.33(1+z) + 8.75. \quad (5)$$

<sup>3</sup>Extinction curves are often expressed with normalization to the value at a certain wavelength  $\lambda_0$ :  $A_{\lambda}/A_{\lambda_0}$  (e.g. Pei, 1992). However, the absolute value of extinction  $A_{\lambda_0}$  is necessary and is unknown for the observed extinction curve in MF12. Reddening ( $A_{\lambda} - A_{\lambda_0}$ ) is easier to derive from the QSO colors.

If we assume that the cosmic extinction up to redshift  $z$  at wavelength  $\lambda_{\text{obs}}$  in the observer’s frame (the optical depth of the cosmic extinction is denoted as  $\tau_{\text{d,cosmo}}(z, \lambda_{\text{obs}})$ ) is dominated by the dust in galaxy halos, we can estimate the dust optical depth per comoving length as  $K_{\text{ext}} = \sigma_{\text{g}} n_{\text{g}} \tau_{\text{d,halo}}(\lambda)$ , where  $\sigma_{\text{g}}$  is the mean geometrical cross-section of galaxy halo,  $n_{\text{g}}$  is the comoving number density of galaxies, and  $\tau_{\text{d,halo}}(\lambda)$  is the mean extinction optical depth of galaxy halo as a function of rest-frame wavelength  $\lambda$ . At the same time, using the mass extinction coefficient,  $\tau_{\text{d,halo}}(\lambda)$  [ $\lambda$  is the rest-frame wavelength, which is related to  $\lambda_{\text{obs}}$  as  $\lambda = \lambda_{\text{obs}}/(1+z)$ ] is estimated as  $\tau_{\text{d,halo}}(\lambda) = \kappa_{\text{ext}}(\lambda) \rho_{\text{d}} l$ , where  $\rho_{\text{d}}$  is the mean dust mass density in galaxy halos and  $l$  is the path length in a halo. Thus, we obtain  $K_{\text{ext}} = \sigma_{\text{g}} n_{\text{g}} \kappa_{\text{ext}}(\lambda) \rho_{\text{d}} l$ . Since  $\sigma_{\text{g}} l$  is the mean volume of galaxy halo,  $\rho_{\text{d}} \sigma_{\text{g}} l$  is reduced to the total dust mass per halo, denoted as  $\langle M_{\text{d,halo}} \rangle$  (Appendix A). After all, using equation (A.6),  $K_{\text{ext}}$  is expressed as

$$K_{\text{ext}}(z, \lambda) = \kappa_{\text{ext}}(\lambda) \langle M_{\text{d,halo}} \rangle n_{\text{g}} = \kappa_{\text{ext}}(\lambda) \rho_{\text{d,halo}}(z). \quad (6)$$

Note that, since we are interested in cosmological-volume properties sampled by random lines of sight, only the mean quantities within a halo is relevant here. Possible clumpiness of dust distribution in halos does not affect our results. This is why the resulting opacity,  $K_{\text{ext}}$ , depends only on the mean dust mass density,  $\rho_{\text{d,halo}}$ .

Finally, the extinction optical depth up to redshift  $z$  at wavelength  $\lambda_{\text{obs}}$  in the observer’s frame,  $\tau_{\text{d,cosmo}}(z, \lambda_{\text{obs}})$ , is estimated as (M10)

$$\tau_{\text{d,cosmo}}(z, \lambda_{\text{obs}}) = \int_0^z K_{\text{ext}} \left( z', \frac{\lambda_{\text{obs}}}{1+z'} \right) \frac{c(1+z')^2}{H(z')} dz', \quad (7)$$

where  $c$  is the light speed, and  $H(z)$  is the Hubble parameter at  $z$ . For the flat Universe,

$$H(z) = H_0 \left[ \Omega_{\text{M}}(1+z)^3 + \Omega_{\Lambda} \right]^{1/2}. \quad (8)$$

## 2.3. Choice of parameter values

The dust abundance in a galaxy halo is regulated by  $\langle \eta \rangle$  (equation 4) in our model. Hereafter, we simply denote  $\langle \eta \rangle$  as  $\eta$  for the brevity of notation. M10 show that the dust mass in a galaxy halo is on average  $\sim 5 \times 10^7 M_{\odot}$ . They also argue that the effective stellar luminosity of their sample is  $0.45 L^*$ . If we assume that the stellar mass of a galaxy with stellar luminosity  $L^*$  is the characteristic mass of the stellar mass function ( $M^* = 10^{11.05} M_{\odot}$ ) derived by Tomczak et al. (2014), the mean stellar mass in M10’s sample is estimated as  $\sim 0.45 M^* = 5 \times 10^{10} M_{\odot}$ . By taking the ratio of the typical dust mass in a halo to the typical stellar mass, we obtain  $\eta \sim 10^{-3}$  for M10’s sample. Peek et al. (2015) derived a similar halo dust mass for sub- $L^*$  galaxies. Thus, we adopt  $\eta = 10^{-3}$  as a fiducial value.

We consider silicate and graphite as representative grain materials that reproduce the extinction curves in nearby galaxies (Draine and Lee, 1984; Weingartner and Draine, 2001). In addition, we adopt amorphous carbon (Zubko et al., 1996), which could be required to reproduce the extinction curves whose

2175 Å bump is not prominent (Nozawa et al., 2015; Hou et al., 2016). We adopt  $s = 3.5, 2.24$  (Weingartner and Draine, 2001) and  $1.81 \text{ g cm}^{-3}$  (Zubko et al., 2004) for the material densities of silicate, graphite, and amorphous carbon, respectively. The extinction coefficient,  $Q_{\text{ext}}(\lambda, a)$ , in equation (1) is calculated using the Mie theory (Bohren and Huffman, 1983) for spherical grains with the optical properties available in the above references. Jones et al. (2013) adopted a different line of models for carbon dust species and also adopted compound (or coagulated) species. However, the present observational data for dust in galaxy halos are not rich enough to distinguish the detailed dust properties; thus, we simply examine the difference between graphite and amorphous carbon as two “representative” carbonaceous species.

### 3. Results

We compare our calculated results with observational data for the reddening curves and the cosmic extinction. Since there are large uncertainties in observational data, we do not attempt any sophisticated fitting procedure, but focus on presenting simple comparisons between our prediction and the observations. However, even with the currently available observational data, we are able to draw some interesting conclusions as we see in this section.

#### 3.1. Reddening curve

The dust grain size is effectively constrained by the reddening curve. Following the assumption in MF12, we trace the reddening in galaxy halos by Mg II absorbers (see also the Introduction). We use the reddening curve derived from the reddening analysis of background QSOs for Mg II absorbers at  $z \sim 1$  and 2 by MF12. We adopt the SDSS  $u, g, r,$  and  $i$  band data, and do not use shorter Galaxy Evolution Explorer (GALEX; Martin et al. 2005) bands, where hydrogen, not dust, dominates the absorption (see fig. 4 in MF12).

As mentioned in Section 2.1, we adopt  $N_{\text{H}} = 10^{19.5} \text{ cm}^{-2}$  for the fiducial value, but considering the uncertainty in  $N_{\text{H}}$  and  $\mathcal{D}$ , we examine an order of magnitude variation of the reddening by changing  $N_{\text{H}}$  between  $10^{19}$  and  $10^{20} \text{ cm}^{-2}$  (but fixing  $\mathcal{D} = 0.006$  because of the degeneracy between  $N_{\text{H}}$  and  $\mathcal{D}$ ). The uncertainty given here is more conservative than that given in MF12.

In Fig. 1, we show the reddening,  $A_{\lambda} - A_i$ , as a function of rest-frame wavelength  $\lambda$  for silicate. We examine three cases for the grain radius:  $a = 0.01, 0.03,$  and  $0.1 \mu\text{m}$ . We find that the observed reddening curves are broadly reproduced with  $a = 0.03 \mu\text{m}$ . If the grain radius is as large as  $a = 0.1 \mu\text{m}$ , the calculated reddening curve is too flat (or  $|A_{\lambda} - A_i|$  is too small) to reproduce the data, which we confirmed to be true also for  $a > 0.1 \mu\text{m}$ . If the grain radius is as small as  $a = 0.01 \mu\text{m}$ , the calculated reddening is too small (especially at  $\lambda > 0.25 \mu\text{m}$ ), simply because  $A_{\lambda}$  is small in the relevant wavelength range (this is true also for  $a < 0.01 \mu\text{m}$ ). Therefore, the grain radii in Mg II absorbers (and probably in galaxy halos) are around  $0.03 \mu\text{m}$  if the main composition is silicate. Silicate grains larger than  $0.1 \mu\text{m}$  or smaller than  $0.01 \mu\text{m}$  are not favored in explaining the reddening curve of Mg II absorbers.

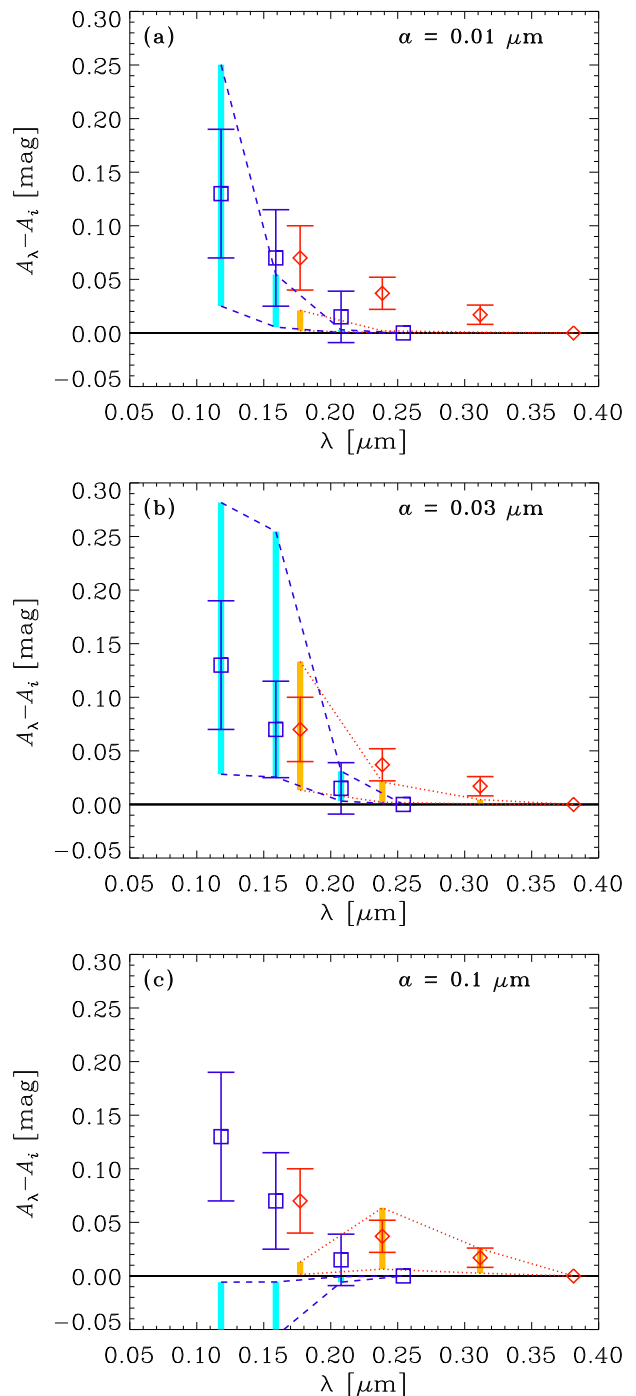


Figure 1: Reddening curves for silicate with grain radii (a)  $a = 0.01 \mu\text{m}$ , (b)  $a = 0.03 \mu\text{m}$ , and (c)  $a = 0.1 \mu\text{m}$  at  $z = 1$  and 2. The orange and light blue bars show the theoretically predicted ranges of  $A_{\lambda} - A_i$  in the SDSS  $u, g,$  and  $r$  bands (the rest-frame wavelengths are shown) at  $z = 1$  and 2, respectively. The red dotted and blue dashed lines connect the upper and lower ranges corresponding to  $N_{\text{H}} = 10^{19} - 10^{20} \text{ cm}^{-2}$  at  $z = 1$  and 2, respectively. The red diamonds and blue squares with error bars show the observed reddening data for Mg II absorbers at  $z = 1$  and 2, respectively, taken from MF12. The error bars are expanded by a factor of 3 relative to those in MF12 for a conservative comparison. If the observational data overlap with the orange and light blue bars, the model is successful. For  $a = 0.01 \mu\text{m}$ , the reddening at  $\lambda > 0.25 \mu\text{m}$  is too small to be clearly seen.

In Fig. 2, we show the reddening curves for graphite. We observe that, because of the prominent 2175 Å bump of small ( $a \lesssim 0.03 \mu\text{m}$ ) graphite grains, the observed reddening is difficult to reproduce with graphite. In particular, the strongly non-monotonic behavior along the wavelength is not supported by the observational data. This is why previous studies such as M10 and MF12 used the SMC extinction curve, which is bumpless, to interpret the extinctions in galaxy halos and Mg II absorbers. For  $a = 0.1 \mu\text{m}$ , the calculated reddening curve is too flat as was also the case with silicate (this is also true for  $a > 0.1 \mu\text{m}$ ). Therefore, graphite is not supported by the observed reddening curves.

Another carbonaceous species, amorphous carbon, does not have such a strong feature; thus, we expect that the observed reddening curves are better explained by amorphous carbon than by graphite. In Fig. 3, we show the reddening curves calculated for amorphous carbon. Because of the weaker bump, as expected, amorphous carbon fits the observed reddening curves better than graphite for  $a = 0.01$  and  $0.03 \mu\text{m}$ . For  $a = 0.1 \mu\text{m}$ , the calculated reddening curve is too flat, as was also the case with graphite. Therefore, a carbonaceous material with a weak feature is marginally accepted by the observed reddening curves if the grain radius is  $a \lesssim 0.03 \mu\text{m}$ .

### 3.2. Cosmic extinction

The second constraint on the dust properties is obtained from the cosmic extinction. For comparison with observational data, we adopt the upper and lower limits for the cosmic extinction at  $z < 2$  compiled in M10. We refer to the appendix in M10 and the references therein for the summary of those data, and only briefly describe them in what follows. Avgoustidis et al. (2009) obtained a constraint on the dust opacity up to  $z \sim 0.5$  by combining the data of the baryon acoustic oscillation and Type Ia SNe. They obtained an upper limit of extinction at the visible wavelength as 0.08 mag. Mörtzell and Goobar (2003) analyzed QSO colors at  $0.5 < z < 2$ , and put an upper limit of  $A_V < 0.2$  mag at  $z \approx 1$ . Ménard et al. (2008) measured the reddening of Mg II absorbers, which are interpreted as residing in halos of  $\sim L^*$  galaxies. Based on their statistical data, M10 estimated the contribution of Mg II absorbers to the cosmic extinction, obtaining  $A_V > 0.009$ ,  $> 0.029$ , and  $> 0.044$  mag at  $z = 0.6$ , 1.3 and 1.8, respectively. Those  $A_V$  values are lower limits because they only count Mg II absorbers. Strictly speaking, their extinction estimates assume that the SMC extinction curve is applicable, which may not be consistent with our adopted wavelength dependence of  $\kappa_V$ . We comment on this issue later in Section 4.1.

We calculate the cosmological extinction  $\tau_{d,\text{cosmo}}(z, \lambda_{\text{obs}})$  (see Section 2.2). Precisely speaking, the observer's frame wavelength  $\lambda_{\text{obs}}$  varies slightly among the observational constraints, but it is always around the V band. We simply represent  $\lambda_{\text{obs}}$  by the V-band wavelength ( $0.55 \mu\text{m}$ ) following M10. This particular choice of wavelength does not affect our discussions below. We present the extinction in units of magnitude by multiplying  $\tau_{d,\text{cosmo}}$  by  $2.5 \log e = 1.086$ .

First, we show the results for various  $\eta$  with a fixed radius  $a = 0.03 \mu\text{m}$  (this grain size is favored by the reddening curve

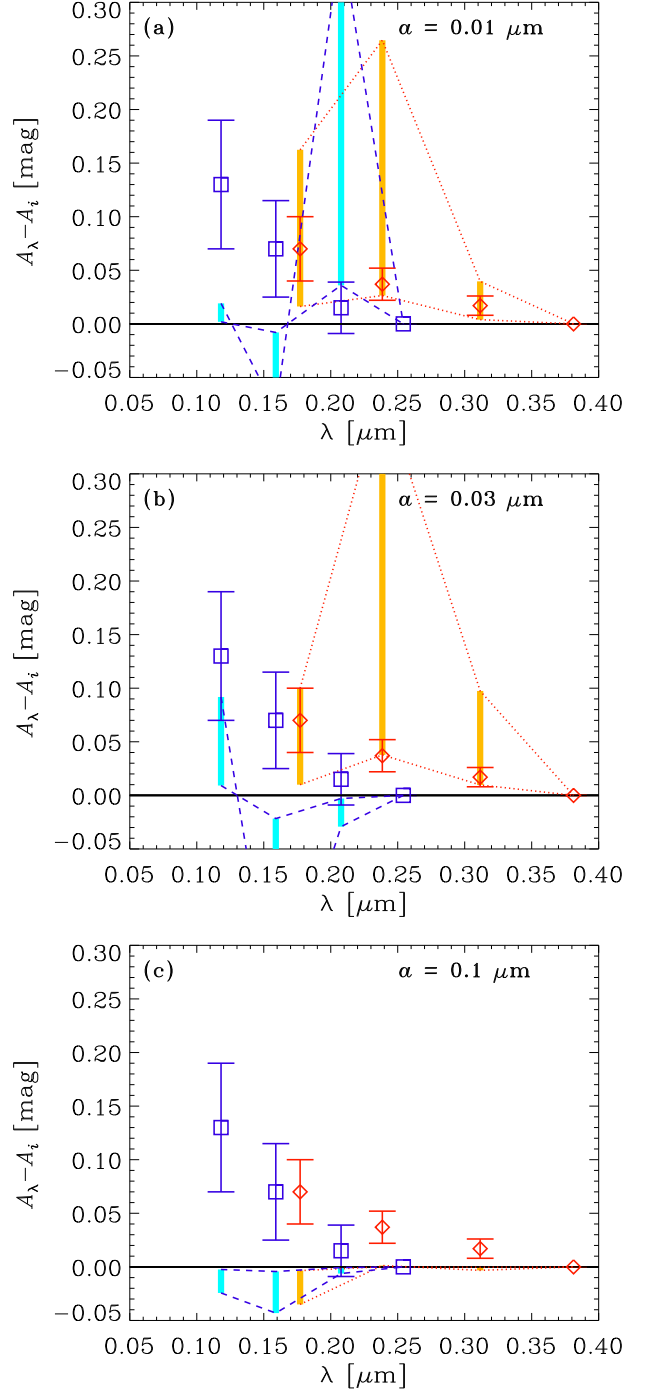


Figure 2: Same as Fig. 1 but for graphite.

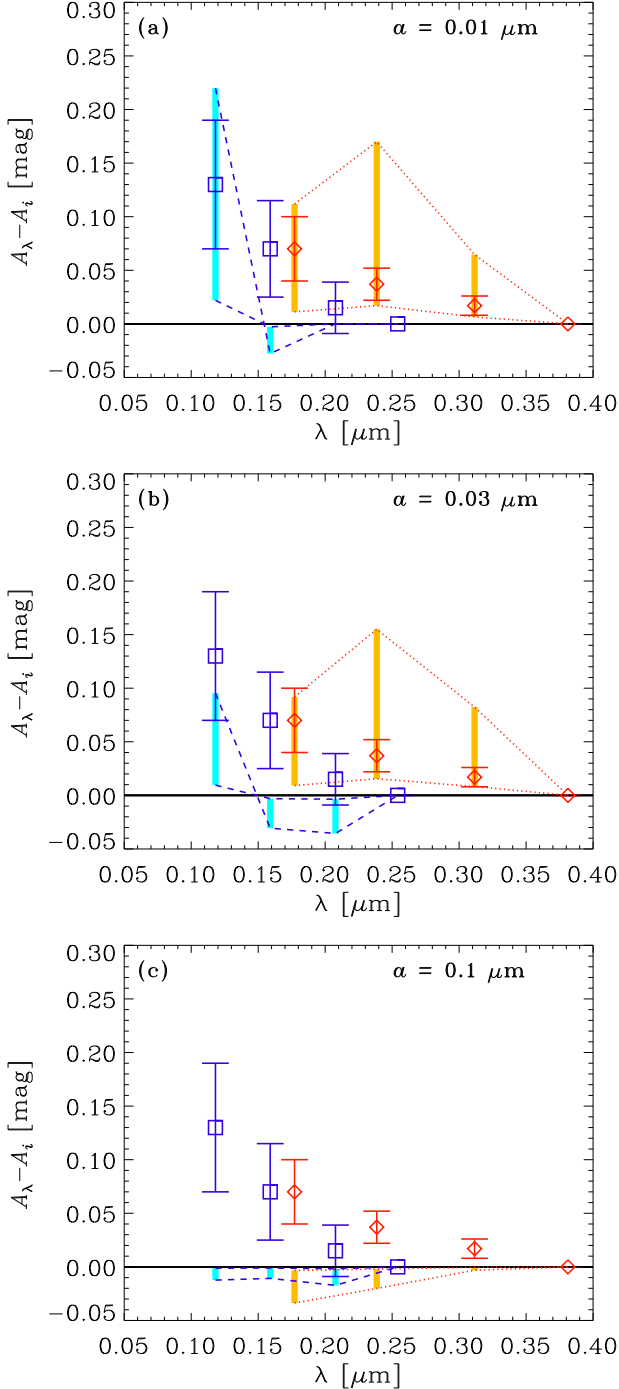


Figure 3: Same as Fig. 1 but for amorphous carbon.

as shown above) in Fig. 4. In this case, the cosmic extinction is simply proportional to  $\eta$ . We observe that, for consistency with the observational constraints,  $\eta > 10^{-2}$  is required for silicate, while the fiducial value  $\eta \sim 10^{-3}$  as suggested above is consistent with the observational constraints for graphite and amorphous carbon.

Next, we calculate the cosmological extinction for various grain radii with a fixed  $\eta = 10^{-3}$  in Fig. 5. As we already discussed above, the extinction of silicate is not large enough to satisfy the observational constraints with  $\eta = 10^{-3}$ . We also find that the silicate extinction is sensitive to the grain radius: for  $a = 0.1 \mu\text{m}$ ,  $\eta$  slightly larger than  $10^{-3}$  is consistent with the observational constraints. Thus, large grains with  $a \sim 0.1 \mu\text{m}$  is favored by the cosmic extinction if the main dust composition is silicate and  $\eta \sim 10^{-3}$ . The extinctions of graphite and amorphous carbon are less sensitive to the grain radius. With the fiducial value of  $\eta (= 10^{-3})$ , graphite and amorphous carbon predict cosmic extinctions consistent with the observational constraints unless the grain radius is  $\gtrsim 0.3 \mu\text{m}$ .

## 4. Discussion

### 4.1. Consistency between reddening and cosmic extinction

We have used two observational constraints: one is the reddening curves observed for Mg II absorbers (assuming that Mg II absorbers trace the medium in galaxy halos), and the other is the cosmic extinction. Below, we summarize the constraint on the grain radius obtained for each grain species in Section 3, and examine if we find grain radii that explain both of the above observational constraints.

For silicate, the reddening curves favor  $a \sim 0.03 \mu\text{m}$ , while the cosmic extinction indicates that we need a halo dust abundance more than  $\sim 10$  times higher than suggested by observation (i.e.,  $\eta \gtrsim 10^{-2}$ ) if  $a \sim 0.03 \mu\text{m}$ . The cosmic extinction is marginally consistent with  $\eta \sim 10^{-3}$  if  $a \sim 0.1 \mu\text{m}$ . Such a large grain size predicts too small a reddening as shown in Fig. 1a. Therefore, if silicate is the main composition, a large amount of dust  $\eta > 10^{-2}$  in galaxy halos is required (in other words, we do not find a consistent grain radius under  $\eta = 10^{-3}$ ).

For graphite, the observed reddening curves are not reproduced well because of the prominent 2175 Å bump. In contrast, the cosmic extinction is consistent with the observational constraints in a broad range of grain radius with the fiducial value of  $\eta (= 10^{-3})$ . Thus, we tried a carbonaceous material without a strong bump in the ultraviolet (UV); that is, amorphous carbon. For amorphous carbon, the reddening curves prefer  $a \lesssim 0.03 \mu\text{m}$ , while the cosmic extinction favors  $a \lesssim 0.1 \mu\text{m}$  under  $\eta = 10^{-3}$ . Thus, small grains with  $a \lesssim 0.03 \mu\text{m}$  is acceptable for both the reddening curves and the cosmic extinction.

In summary, depending on the main dust composition, there are two lines of “solutions” for the consistency between the reddening curves and the cosmic extinction: if the main material is silicate, grains should have radii  $\sim 0.03 \mu\text{m}$  but a higher dust abundance ( $\eta > 10^{-2}$ ) in galaxy halos than suggested by the observations is required. If the main component of dust in galaxy halos is carbonaceous dust, it should not have a strong bump

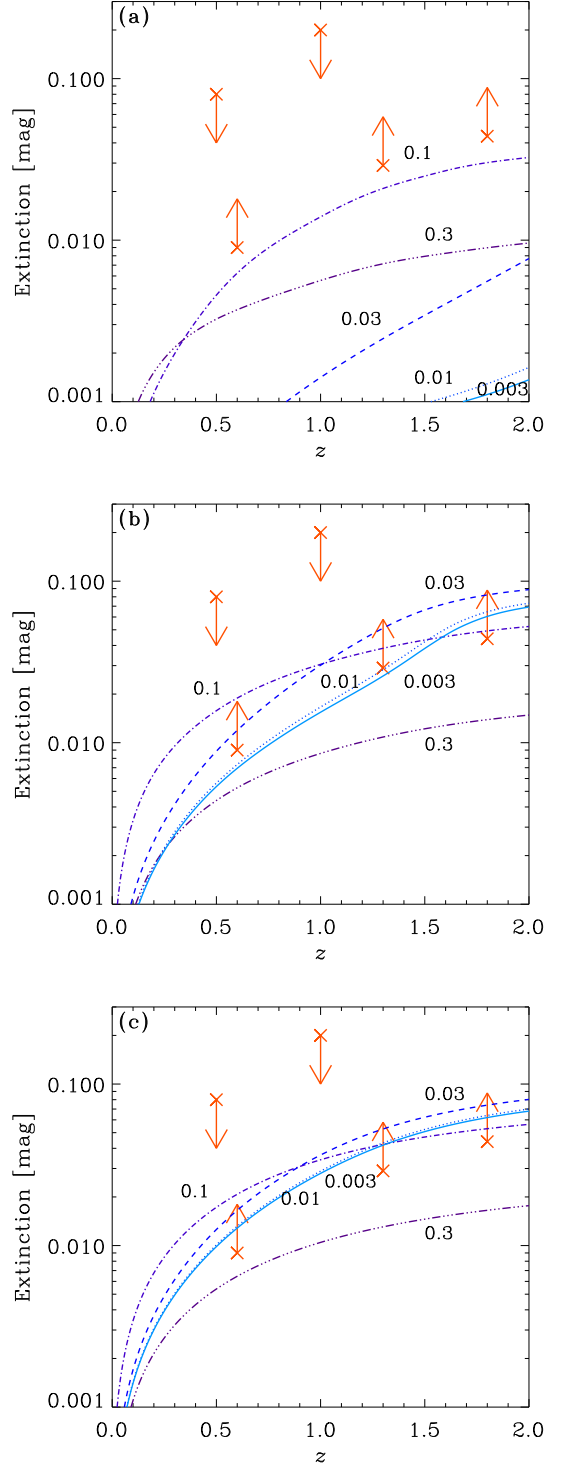
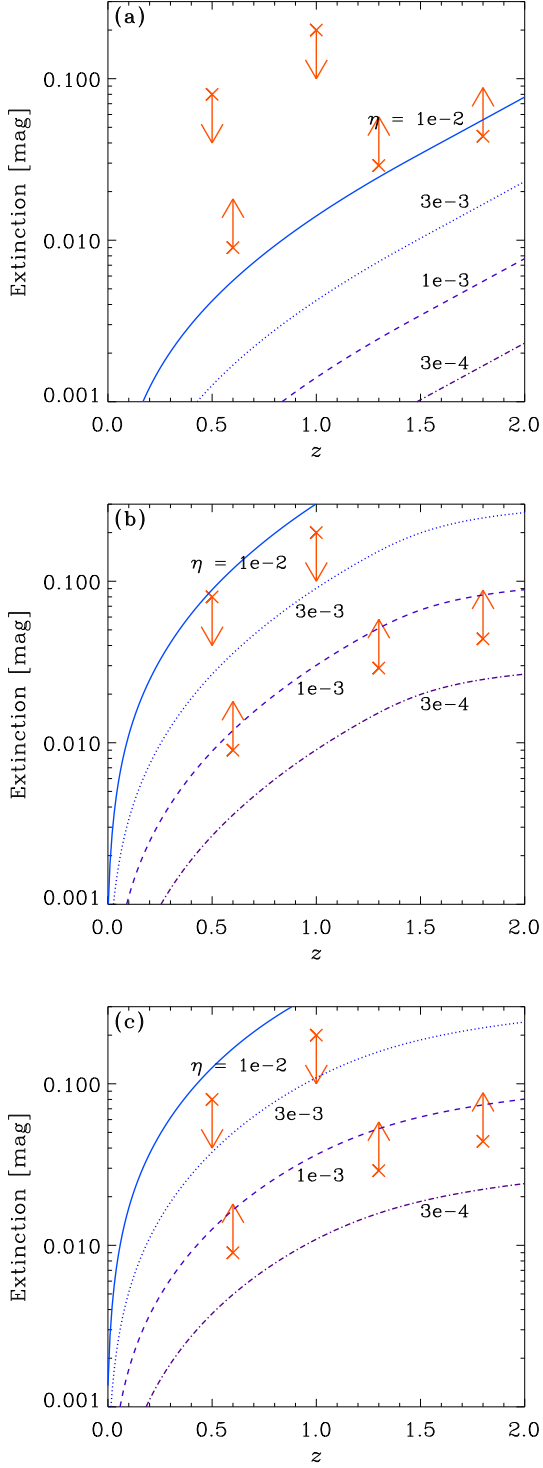


Figure 4: Extinction as a function of redshift (cosmic extinction) for various  $\eta$  (dust abundance in the halo relative to the stellar mass) with a fixed grain size of  $a = 0.03 \mu\text{m}$ . Panels (a), (b), and (c) show silicate, graphite and amorphous carbon. The solid, dotted, dashed, and dot-dashed lines present the results for  $\eta = 10^{-2}$ ,  $3 \times 10^{-3}$ ,  $10^{-3}$ , and  $3 \times 10^{-4}$ , respectively. Upper (downward arrows) and lower (upward arrows) limits at various redshifts are taken from M10 (see the references therein).

Figure 5: Same as Fig. 4 but for various grain radii with a fixed  $\eta = 10^{-3}$ . The solid, dotted, dashed, dot-dashed, and dot-dot-dot-dashed lines show the results for  $a = 0.003, 0.01, 0.03, 0.1, \text{ and } 0.3 \mu\text{m}$ , respectively.

in the UV and should have grain radii  $a \lesssim 0.03 \mu\text{m}$  under the fiducial value of  $\eta = 10^{-3}$ .

Precisely speaking, the observational lower limits on the cosmic extinction in Figs. 4 and 5 have been derived using the SMC extinction curve. If large grains ( $a \gtrsim 0.1 \mu\text{m}$ ), whose extinction curve is significantly flatter than the SMC curve, are the main component of dust in galaxy halos, more dust is necessary to reproduce the same amount of reddening. That is, the observational lower limits shown in Figs. 4 and 5 are raised if the grain size is large. Therefore, the discrepancy between our theoretical predictions for  $a \gtrsim 0.1 \mu\text{m}$  and the lower limits become larger in Fig. 5a. Such large grains are, however, not favored by the reddening constraints obtained in Section 3.1.

#### 4.2. Effects of grain size distribution

In the above, we have simply assumed that all the grains have a single radius. This radius is interpreted as the typical radius of grains which dominate the extinction opacity. This approach is useful because constraining the grain size distribution only with sparse wavelength sampling of a reddening curve is a highly degenerate problem. It is expected that the above conclusion on the necessity of small ( $a \lesssim 0.03 \mu\text{m}$ ) grains in reproducing the reddening curve is robust even if we consider a grain size distribution.

Although the full grain size distribution is impossible to determine, it is worth examining the effect of grain size distribution on the conclusion. In particular, we focus on examining if small ( $a \lesssim 0.03 \mu\text{m}$ ) grains are required robustly. To concentrate on the existence of small grains, we fix the maximum grain radius,  $a_{\text{max}}$ , and the functional form of the grain size distribution but move the minimum grain radius,  $a_{\text{min}}$ :

$$n(a) = Ca^{-3.5} \quad (a_{\text{min}} \leq a \leq a_{\text{max}}), \quad (9)$$

where  $C$  is the normalizing constant (but as we show below,  $C$  is not important). This power-law form is appropriate for the Milky Way dust (Mathis et al., 1977, hereafter MRN). Although there is no physical reason that this functional form is applicable to the IGM/CGM dust, we simply adopt this form to examine the effect of small grains ( $a_{\text{min}}$ ). We adopt  $a_{\text{max}} = 0.25 \mu\text{m}$  according to MRN, while we vary  $a_{\text{min}} = 0.01, 0.03,$  and  $0.1 \mu\text{m}$ .

We extend the formulation in Section 2.1 by considering the grain size distribution. The mass extinction coefficient is expressed instead of equation (1) as

$$\kappa_{\text{ext}}(\lambda) = \frac{\int_{a_{\text{min}}}^{a_{\text{max}}} \pi a^2 Q_{\text{ext}}(\lambda, a) n(a) da}{\int_{a_{\text{min}}}^{a_{\text{max}}} \frac{4}{3} \pi a^3 s n(a) da}. \quad (10)$$

Here the above normalization constant  $C$  cancels out.

In Fig. 6, we show the reddening curve for silicate with the above grain size distribution. Compared with Fig. 1, the steepness of the reddening curve is moderate for  $a_{\text{min}} = 0.01$  and  $0.03 \mu\text{m}$  because of the contamination of large grains. Nevertheless, the theoretical reddening curves are broadly consistent with the observations if  $a_{\text{min}} \leq 0.03 \mu\text{m}$ . As shown in Fig. 1, silicate grains with  $a \sim 0.01 \mu\text{m}$  have too small extinction, so the major contribution comes from grains with

$a \sim 0.03 \mu\text{m}$  for even if  $a_{\text{min}} = 0.01 \mu\text{m}$ . The reddening curves with  $a_{\text{min}} = 0.1 \mu\text{m}$  is too flat to explain the observed curves. Therefore, we strengthen the conclusion that, if the main composition is silicate, small grains with  $a \sim 0.03 \mu\text{m}$  is necessary to explain the observed reddening curves in Mg II absorbers.

In Fig. 7, we show the results for graphite. Because of the contamination of large grains, the bump feature is moderate compared with Fig. 2; however, the non-monotonic behavior affected by the bump still remains if  $a_{\text{min}} \lesssim 0.03 \mu\text{m}$ . If the minimum grain size is as large as  $\sim 0.1 \mu\text{m}$ , the reddening curve is too flat to explain the observations. Therefore, graphite is still not favored even if we consider the effect of grain size distribution.

In Fig. 8, we show the reddening curves for amorphous carbon. As expected, the strong bump is effectively eliminated. However, the calculated reddening curves are too flat to explain the observations even with  $a_{\text{min}} = 0.01 \mu\text{m}$  because of the contamination of large grains. Therefore, if the major component of dust is amorphous carbon, it is required that most grains have  $a \lesssim 0.03 \mu\text{m}$ .

The conclusions derived with a single grain radius are not altered as long as the reddening curve is concerned: if the main composition is silicate, small grains with  $a \lesssim 0.03 \mu\text{m}$  are required (i.e.,  $a_{\text{min}} \lesssim 0.03 \mu\text{m}$ ). If the main composition is carbonaceous dust, the grain size distribution should be biased to small sizes ( $a \lesssim 0.03 \mu\text{m}$ ).

In Fig. 9, we also plot the cosmic extinction with the effect of grain size distribution. We adopt  $\eta = 10^{-3}$ . Compared with Fig. 5, the variation of cosmic extinction among various  $a_{\text{min}}$  is smaller. For silicate with  $a_{\text{min}} = 0.03 \mu\text{m}$ , which produces a consistent reddening curve with observations (Fig. 6), the theoretical cosmic extinction is 3 times smaller than the observational lower limits. This discrepancy (3 times) is smaller than the discrepancy seen in the single-size case with  $a = 0.03 \mu\text{m}$  (10 times; Fig. 5a). This means that, if we take the grain size distribution into account, we find a solution that explains both the reddening curves and the cosmic extinction with  $\eta \gtrsim 3 \times 10^{-3}$ . For graphite and amorphous carbon, the calculated cosmic extinction is consistent with the observational constraints.

In summary, the conclusions under the single-radius treatment above do not change significantly even if we consider the grain size distribution: (i) For silicate, inclusion of small  $a_{\text{min}} \lesssim 0.03 \mu\text{m}$  is favored, and a larger dust abundance ( $\eta \gtrsim 3 \times 10^{-3}$ ) than suggested by observations is required. (ii) For carbonaceous dust (amorphous carbon), small grains with  $a \sim 0.03 \mu\text{m}$  should be dominant.

#### 4.3. Comparison with other theoretical studies

Recently, there have been some cosmological simulations and semi-analytic models that calculate dust formation in galaxies and subsequent dust transport into galaxy halos or intergalactic space (McKinnon et al., 2016, 2017; Popping et al., 2017). McKinnon et al. (2016) showed that the radial profile of dust surface density in the galaxy halo can be roughly consistent with M10's observational data, depending on the stellar feedback model adopted (see also Aoyama et al., 2018).

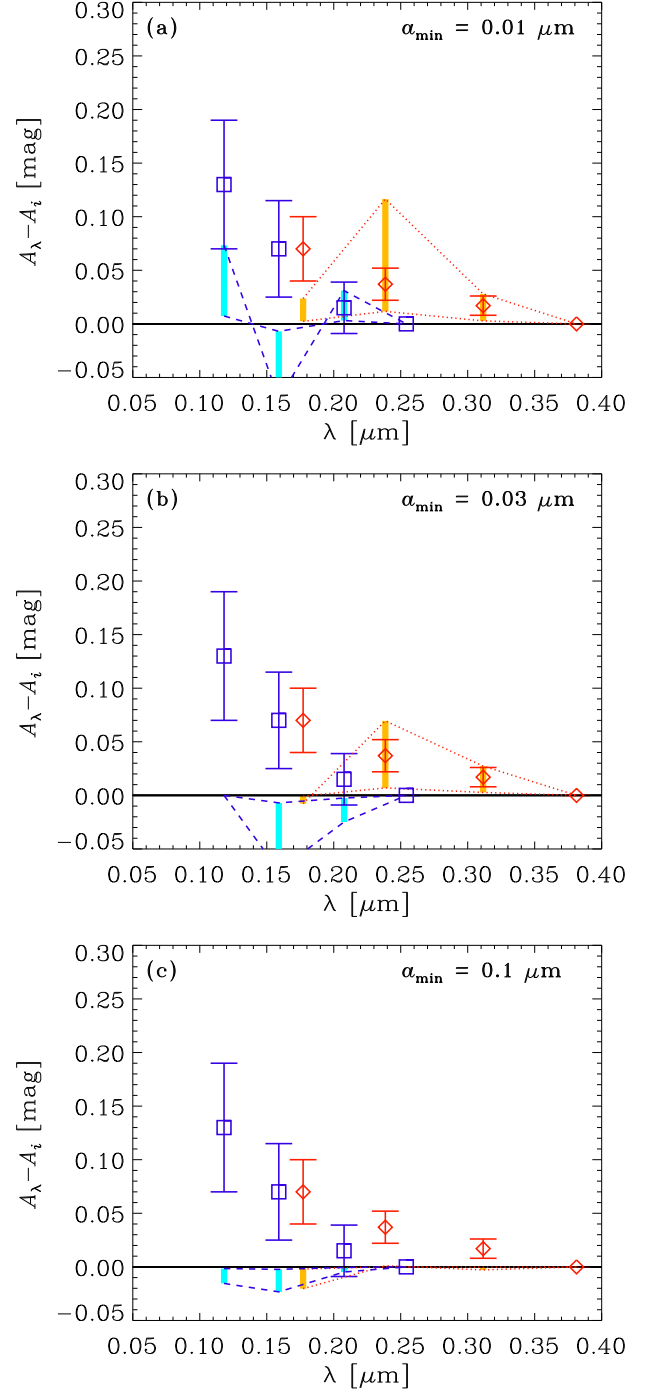
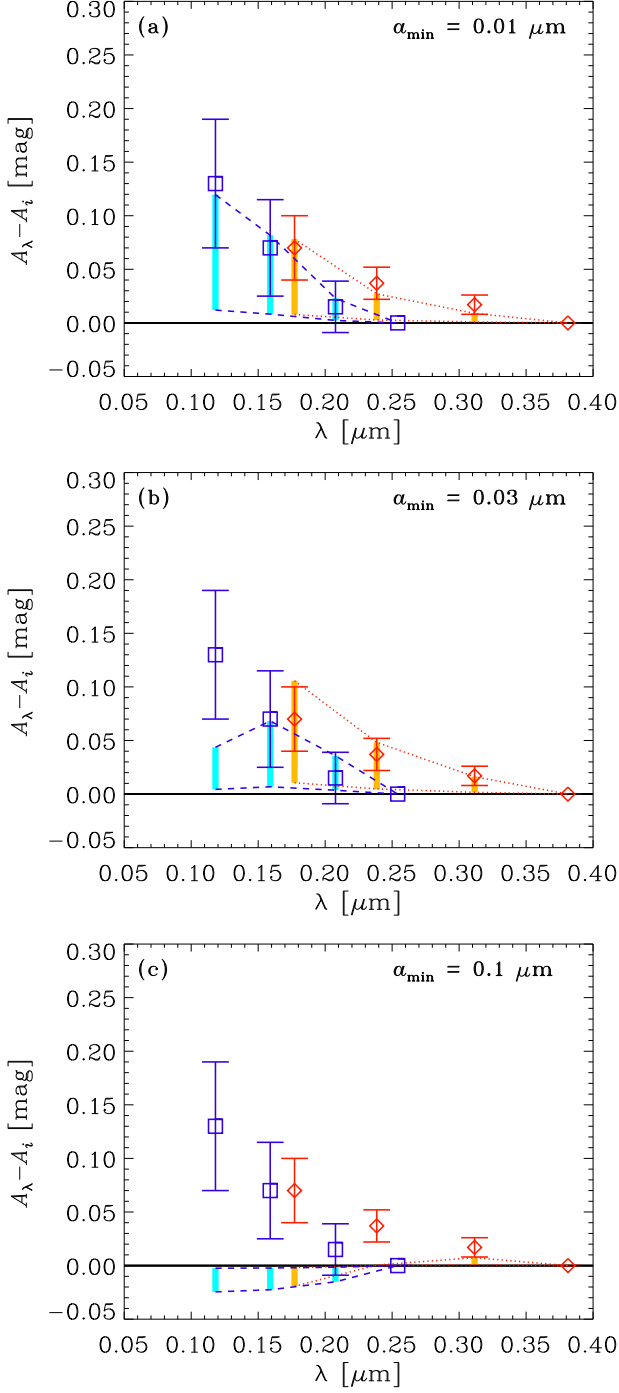


Figure 6: Same as Fig. 1 but including the effect of grain size distribution (equation 9 with  $a_{\max} = 0.25 \mu\text{m}$ ) for silicate. The minimum grain radius is varied as (a)  $a_{\min} = 0.01 \mu\text{m}$ , (b)  $a_{\min} = 0.03 \mu\text{m}$ , and (c)  $a_{\min} = 0.1 \mu\text{m}$ .

Figure 7: Same as Fig. 6 but for graphite.

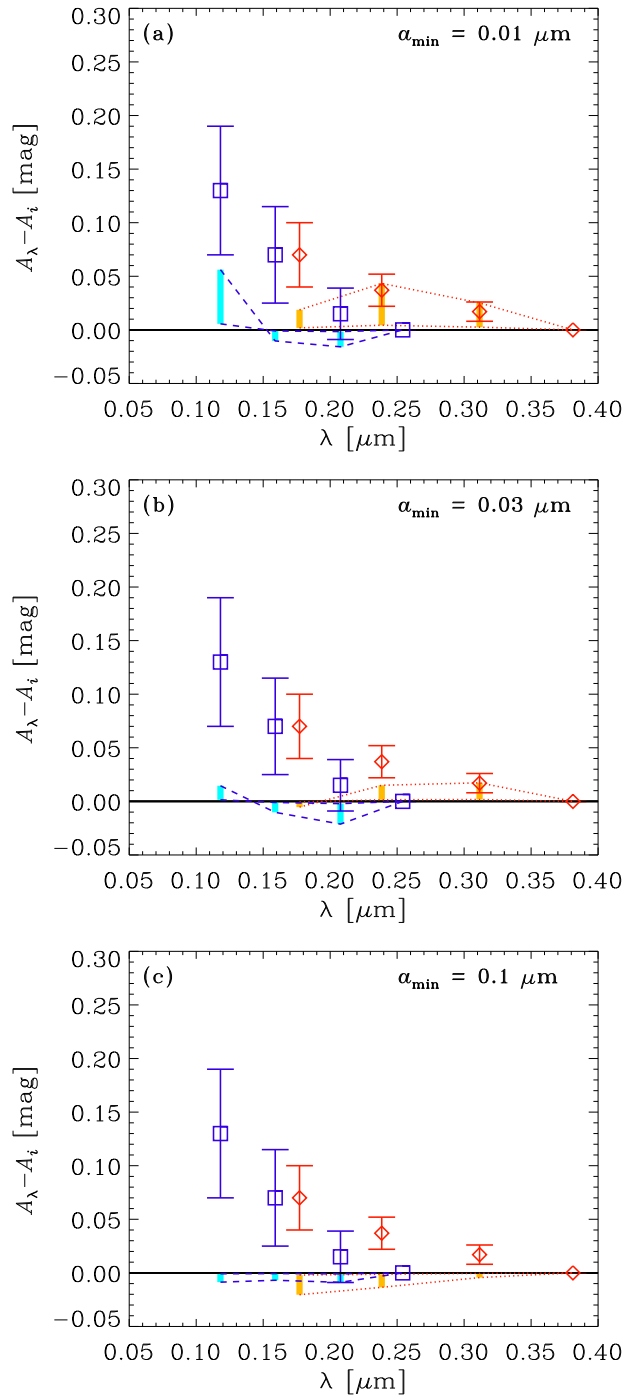


Figure 8: Same as Fig. 6 but for amorphous carbon.

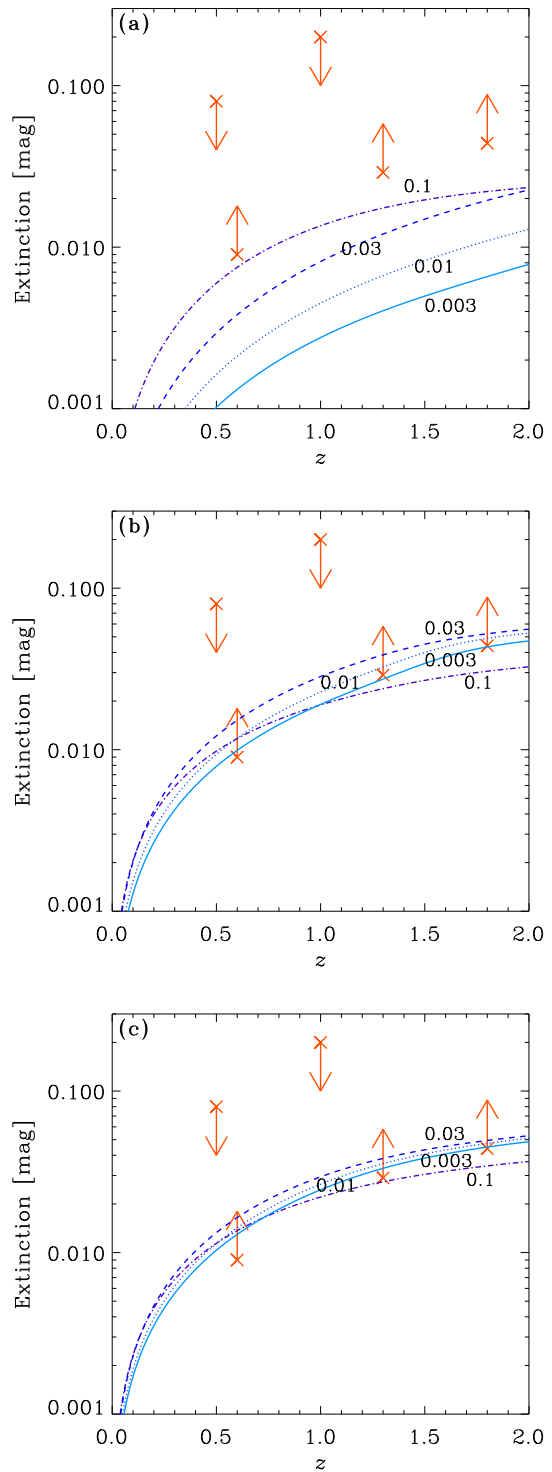


Figure 9: Same as Fig. 5 but including the effect of grain size distribution. The solid, dotted, dashed, and dot-dashed lines show the results for  $a_{\min} = 0.003, 0.01, 0.03,$  and  $0.1 \mu\text{m}$ , respectively.

Popping et al. (2017), using their semi-analytic model, showed that the galaxy halo component contains a comparable amount of dust to the ISM component. Zu et al. (2011) used a cosmological hydrodynamics simulation and reproduced the radial distribution of dust in galaxy halos by assuming that dust traces the metals. They also showed the dust abundance in galaxy halos is sensitive to the stellar feedback model. Therefore, it is still a challenge for theoretical models to reproduce such a large dust abundance in galaxy halos as observed by M10.

Hydrodynamic simulations with dust enrichment by Aoyama et al. (2017, 2018) and Hou et al. (2017) treat information on grain size distribution represented by the abundance of large and small grains. Hou et al. (2017) and Aoyama et al. (2018) show that the grains in galaxy halos are biased to large ( $a > 0.03 \mu\text{m}$ ) grains. In contrast, as shown above, the reddening curves of Mg II absorbers at  $z \sim 1$  and 2 indicate the dominance of small ( $a \lesssim 0.03 \mu\text{m}$ ) grains. Thus, there is a tension in the grain size between the above simulations and the observed reddening curves. However, the above two simulations did not include dust transport by radiation pressure, which could be important as a mechanism of outflow (Murray et al., 2011). Ferrara et al. (1991) and Bianchi and Ferrara (2005) show that grains with  $a \sim 0.03\text{--}0.3 \mu\text{m}$  can be dynamically decoupled from gas and transported to the galaxy halo, but that the radiation pressure has no reason of preferentially transporting grains with  $a \lesssim 0.03 \mu\text{m}$ .

It may be possible that small grains are produced *in situ* in Mg II absorbers. Some authors argue that Mg II absorbers are associated with outflow induced by active star formation (Norman et al., 1996; Bond et al., 2001). Because of a high velocity of outflow, shock or high-velocity turbulence could be induced in the wind. Both shock (Jones et al., 1996) and turbulence (Yan et al., 2004; Hirashita and Yan, 2009) are considered as mechanisms of inducing grain shattering. Therefore, grains may be shattered in the outflows. It is suggested that Mg II absorbers has a spatial scale as small as 30 pc (Lan and Fukugita, 2017). Since the above simulations are not capable of resolving such a small-scale structure, shattering in outflowing gas was not successfully treated. In the future, it may be desirable to investigate the possibility of shattering in outflows using a high-resolution simulations that are capable of resolving the internal structures in the outflowing gas.

## 5. Conclusion

We investigate the abundance and properties of the dust in galaxy halos using available observations in the literature. There are two major sets of data: reddening curves and cosmic extinction. The reddening curves are derived by assuming that Mg II absorbers trace the medium in galaxy halos. From the reddening curves, we show that the typical grain radius is  $a \sim 0.03 \mu\text{m}$  for silicate. Graphite is not consistent with the observed reddening curve because of its strong 2175 Å bump. Using amorphous carbon improves the fit to the reddening. For amorphous carbon,  $a \lesssim 0.03 \mu\text{m}$  is supported by the reddening curves.

The observational constraints on the cosmic extinction suggest that the grain radius be  $a \lesssim 0.1 \mu\text{m}$  for carbonaceous dust if the halo dust abundance relative to the stellar mass is  $\eta = 10^{-3}$  as suggested by M10. For silicate, if  $\eta = 10^{-3}$ , the cosmic extinction is significantly underestimated and only  $a \sim 0.1 \mu\text{m}$  is marginally consistent with the observational lower limits. In other words, silicate favors a higher dust abundance in galaxy halos such as  $\eta \gtrsim 10^{-2}$  if we adopt  $a \sim 0.03 \mu\text{m}$  suggested by the reddening curves. The constraint on  $\eta$  becomes milder ( $\eta \gtrsim 3 \times 10^{-3}$ ) if we take a grain size distribution into account, but the value of  $\eta$  is still larger than the fiducial value. Thus, if the main dust composition in galaxy halos is silicate, there is a tension in the grain size between the constraint from the reddening and that from the cosmic extinction. For carbonaceous dust (amorphous carbon), those two constraints indicate  $a \lesssim 0.03 \mu\text{m}$ . The requirement of small grains with  $a \lesssim 0.03 \mu\text{m}$  is robustly concluded even if we consider grain size distribution.

The favored grain radii ( $a \lesssim 0.03 \mu\text{m}$ ) in galaxy halos are not in line with numerical simulations by Hou et al. (2017) and Aoyama et al. (2018). In their scenario, the halo dust is dominated by large ( $a > 0.03 \mu\text{m}$ ) grains originating from stars because the dust tends to be ejected by stellar feedback before being significantly processed in the ISM by shattering and accretion. Although the above simulations do not include the effect of radiation pressure, there is no physical reason that small grains are selectively transported by radiation pressure. We point out a possibility of shattering in the outflow driven by stellar feedback, but a high resolution simulation is necessary to examine whether or not this happens.

## Acknowledgment

We are grateful to S. Aoyama, K. Nagamine, K.-C. Hou, S. Bianchi, and the anonymous referee for their useful discussions and comments. HH thanks the Ministry of Science and Technology for support through grant MOST 105-2112-M-001-027-MY3 and MOST 107-2923-M-001-003-MY3.

## Appendix A. Comoving mass densities

The comoving stellar mass density,  $\rho_{\text{star}}$ , is estimated using the stellar mass function as

$$\rho_{\text{star}} = \int M_{\text{star}} \Phi(M_{\text{star}}) dM_{\text{star}}, \quad (\text{A.1})$$

while the comoving halo dust mass density,  $\rho_{\text{d,halo}}$ , is estimated as

$$\rho_{\text{d,halo}} = \int M_{\text{d,halo}} \Phi(M_{\text{star}}) dM_{\text{star}}. \quad (\text{A.2})$$

We also evaluate the comoving number density of galaxies:

$$n_{\text{g}} = \int \Phi(M_{\text{star}}) dM_{\text{star}}. \quad (\text{A.3})$$

Now we define the averaged halo dust-to-stellar mass ratio,  $\langle \eta \rangle$  as

$$\begin{aligned} \langle \eta \rangle &= \int M_{\text{d,halo}} \Phi(M_{\text{star}}) dM_{\text{star}} \bigg/ \int M_{\text{star}} \Phi(M_{\text{star}}) dM_{\text{star}} \\ &= \int \eta M_{\text{star}} \Phi(M_{\text{star}}) dM_{\text{star}} \bigg/ \int M_{\text{star}} \Phi(M_{\text{star}}) dM_{\text{star}} . \end{aligned} \quad (\text{A.4})$$

Using equations (A.1), (A.2), and (A.4), we obtain equation (4).

We also define the average halo dust mass as

$$\langle M_{\text{d,halo}} \rangle = \int M_{\text{d,halo}} \Phi(M_{\text{star}}) dM_{\text{star}} \bigg/ \int \Phi(M_{\text{star}}) dM_{\text{star}} . \quad (\text{A.5})$$

Using equations (A.2), (A.3) and (A.5), we obtain

$$\rho_{\text{d,halo}} = n_{\text{g}} \langle M_{\text{d,halo}} \rangle . \quad (\text{A.6})$$

## References

- Aguirre, A., 1999. Intergalactic Dust and Observations of Type IA Supernovae. *Astrophys. J.* 525, 583–593.
- Aoyama, S., Hou, K.-C., Hirashita, H., Nagamine, K., Shimizu, I., 2018. Cosmological simulation with dust formation and destruction. ArXiv e-prints.
- Aoyama, S., Hou, K.-C., Shimizu, I., Hirashita, H., Todoroki, K., Choi, J.-H., Nagamine, K., 2017. Galaxy simulation with dust formation and destruction. *Mon. Not. R. Astron. Soc.* 466, 105–121.
- Asano, R. S., Takeuchi, T. T., Hirashita, H., Nozawa, T., 2013. What determines the grain size distribution in galaxies? *Mon. Not. R. Astron. Soc.* 432, 637–652.
- Avgoustidis, A., Verde, L., Jimenez, R., 2009. Consistency among distance measurements: transparency, BAO scale and accelerated expansion. *Journal of Cosmology and Astroparticle Physics* 6, 012.
- Bekki, K., 2015. Dust-regulated galaxy formation and evolution: a new chemical dynamical model with live dust particles. *Mon. Not. R. Astron. Soc.* 449, 1625–1649.
- Bianchi, S., Ferrara, A., 2005. Intergalactic medium metal enrichment through dust sputtering. *Mon. Not. R. Astron. Soc.* 358, 379–396.
- Bohren, C. F., Huffman, D. R., 1983. *Absorption and Scattering of Light by Small Particles*. Wiley.
- Bond, N. A., Churchill, C. W., Charlton, J. C., Vogt, S. S., 2001. High-Redshift Superwinds as the Source of the Strongest Mg II Absorbers: A Feasibility Analysis. *Astrophys. J.* 562, 641–648.
- Bouché, N., Murphy, M. T., Péroux, C., Davies, R., Eisenhauer, F., Förster Schreiber, N. M., Tacconi, L., 2007. The SINFONI Mg II Program for Line Emitters (SIMPLE): Discovering Starbursts near QSO Sight Lines. *Astrophys. J.* 669, L5–L8.
- Draine, B. T., Lee, H. M., 1984. Optical properties of interstellar graphite and silicate grains. *Astrophys. J.* 285, 89–108.
- Evans, A., 1994. *The Dusty Universe*. Wiley.
- Ferrara, A., Ferrini, F., Barsella, B., Franco, J., 1991. Evolution of dust grains through a hot gaseous halo. *Astrophys. J.* 381, 137–146.
- Hildebrand, R. H., 1983. The Determination of Cloud Masses and Dust Characteristics from Submillimetre Thermal Emission. *Quarterly J. of the R. Astron. Soc.* 24, 267.
- Hirashita, H., Yan, H., 2009. Shattering and coagulation of dust grains in interstellar turbulence. *Mon. Not. R. Astron. Soc.* 394, 1061–1074.
- Hou, K.-C., Hirashita, H., Michałowski, M. J., 2016. Dust evolution processes constrained by extinction curves in nearby galaxies. *Publ. Astron. Soc. Japan* 68, 94.
- Hou, K.-C., Hirashita, H., Nagamine, K., Aoyama, S., Shimizu, I., 2017. Evolution of dust extinction curves in galaxy simulation. *Mon. Not. R. Astron. Soc.* 469, 870–885.
- Inoue, A. K., Kamaya, H., 2003. Constraint on intergalactic dust from thermal history of intergalactic medium. *Mon. Not. R. Astron. Soc.* 341, L7–L11.
- Inoue, A. K., Kamaya, H., 2004. Amount of intergalactic dust: constraints from distant supernovae and the thermal history of the intergalactic medium. *Mon. Not. R. Astron. Soc.* 350, 729–744.
- Inoue, A. K., Kamaya, H., 2010. Intergalactic dust and its photoelectric heating. *Earth, Planets, and Space* 62, 69–79.
- Jenkins, E. B., 2009. A Unified Representation of Gas-Phase Element Depletions in the Interstellar Medium. *Astrophys. J.* 700, 1299–1348.
- Jones, A. P., Fanciullo, L., Köhler, M., Verstraete, L., Guillet, V., Bocchio, M., Ysard, N., 2013. The evolution of amorphous hydrocarbons in the ISM: dust modelling from a new vantage point. *Astron. Astrophys.* 558, A62.
- Jones, A. P., Tielens, A. G. G. M., Hollenbach, D. J., 1996. Grain Shattering in Shocks: The Interstellar Grain Size Distribution. *Astrophys. J.* 469, 740.
- Kereš, D., Katz, N., Weinberg, D. H., Davé, R., 2005. How do galaxies get their gas? *Mon. Not. R. Astron. Soc.* 363, 2–28.
- Lan, T.-W., Fukugita, M., 2017. Mg II Absorbers: Metallicity Evolution and Cloud Morphology. *Astrophys. J.* 850, 156.
- Martin, D. C., Fanson, J., Schiminovich, D., Morrissey, P., Friedman, P. G., Barlow, T. A., Conrow, T., Grange, R., Jelinsky, P. N., Milliard, B., Siegmund, O. H. W., Bianchi, L., Byun, Y.-I., Donas, J., Forster, K., Heckman, T. M., Lee, Y.-W., Madore, B. F., Malina, R. F., Neff, S. G., Rich, R. M., Small, T., Surber, F., Szalay, A. S., Welsh, B., Wyder, T. K., 2005. The Galaxy Evolution Explorer: A Space Ultraviolet Survey Mission. *Astrophys. J.* 619, L1–L6.
- Masaki, S., Yoshida, N., 2012. Distribution of dust around galaxies: an analytic model. *Mon. Not. R. Astron. Soc.* 423, L117–L121.
- Mathis, J. S., Rumpl, W., Nordsieck, K. H., Oct. 1977. The size distribution of interstellar grains. *Astrophys. J.* 217, 425–433.
- McKinnon, R., Torrey, P., Vogelsberger, M., 2016. Dust formation in Milky Way-like galaxies. *Mon. Not. R. Astron. Soc.* 457, 3775–3800.
- McKinnon, R., Torrey, P., Vogelsberger, M., Hayward, C. C., Marinacci, F., 2017. Simulating the dust content of galaxies: successes and failures. *Mon. Not. R. Astron. Soc.* 468, 1505–1521.
- Ménard, B., Chelouche, D., 2009. On the HI content, dust-to-gas ratio and nature of MgII absorbers. *Mon. Not. R. Astron. Soc.* 393, 808–815.
- Ménard, B., Fukugita, M., 2012. Cosmic Dust in Mg II Absorbers. *Astrophys. J.* 754, 116.
- Ménard, B., Nestor, D., Turnshek, D., Quider, A., Richards, G., Chelouche, D., Rao, S., 2008. Lensing, reddening and extinction effects of MgII absorbers from  $z = 0.4$  to  $z = 2$ . *Mon. Not. R. Astron. Soc.* 385, 1053–1066.
- Ménard, B., Scranton, R., Fukugita, M., Richards, G., 2010. Measuring the galaxy-mass and galaxy-dust correlations through magnification and reddening. *Mon. Not. R. Astron. Soc.* 405, 1025–1039.
- Mörtzell, E., Goobar, A., 2003. Constraints on intergalactic dust from quasar colours. *Journal of Cosmology and Astroparticle Physics* 9, 009.
- Murray, N., Ménard, B., Thompson, T. A., 2011. Radiation Pressure from Massive Star Clusters as a Launching Mechanism for Super-galactic Winds. *Astrophys. J.* 735, 66.
- Norman, C. A., Bowen, D. V., Heckman, T., Blades, C., Danly, L., 1996. Hubble Space Telescope Observations of QSO Absorption Lines Associated with Starburst Galaxy Outflows. *Astrophys. J.* 472, 73.
- Nozawa, T., Asano, R. S., Hirashita, H., Takeuchi, T. T., 2015. Evolution of grain size distribution in high-redshift dusty quasars: integrating large amounts of dust and unusual extinction curves. *Mon. Not. R. Astron. Soc.* 447, L16–L20.
- Peek, J. E. G., Ménard, B., Corrales, L., 2015. Dust in the Circumgalactic Medium of Low-redshift Galaxies. *Astrophys. J.* 813, 7.
- Pei, Y. C., 1992. Interstellar dust from the Milky Way to the Magellanic Clouds. *Astrophys. J.* 395, 130–139.
- Popping, G., Somerville, R. S., Galametz, M., 2017. The dust content of galaxies from  $z = 0$  to  $z = 9$ . *Mon. Not. R. Astron. Soc.* 471, 3152–3185.
- Steidel, C. C., Dickinson, M., Meyer, D. M., Adelberger, K. L., Sembach, K. R., 1997. Quasar Absorbing Galaxies at  $z \lesssim 1$ : Deep Imaging and Spectroscopy in the Field of 3C 336. *Astrophys. J.* 480, 568–588.
- Tomczak, A. R., Quadri, R. F., Tran, K.-V. H., Labbé, I., Straatman, C. M. S., Papovich, C., Glazebrook, K., Allen, R., Brammer, G. B., Kacprzak, G. G., Kawinwanichakij, L., Kelson, D. D., McCarthy, P. J., Mehtens, N., Monson, A. J., Persson, S. E., Spitler, L. R., Tilvi, V., van Dokkum, P., 2014. Galaxy Stellar Mass Functions from ZFOURGE/CANDELS: An Excess of Low-mass Galaxies since  $z = 2$  and the Rapid Buildup of Quiescent Galaxies. *Astrophys. J.* 783, 85.
- Tremonti, C. A., Moustakas, J., Diamond-Stanic, A. M., 2007. The Discovery of  $1000 \text{ km s}^{-1}$  Outflows in Massive Poststarburst Galaxies at  $z = 0.6$ . *Astrophys. J.* 663, L77–L80.
- Veilleux, S., Cecil, G., Bland-Hawthorn, J., 2005. Galactic Winds. *Ann. Rev.*

- Astron. Astrophys. 43, 769–826.
- Weingartner, J. C., Draine, B. T., 2001. Dust Grain-Size Distributions and Extinction in the Milky Way, Large Magellanic Cloud, and Small Magellanic Cloud. *Astrophys. J.* 548, 296–309.
- Yan, H., Lazarian, A., Draine, B. T., 2004. Dust Dynamics in Compressible Magnetohydrodynamic Turbulence. *Astrophys. J.* 616, 895–911.
- York, D. G., et al., 2000. The Sloan Digital Sky Survey: Technical Summary. *Astron. J.* 120, 1579–1587.
- York, D. G., Khare, P., Vanden Berk, D., Kulkarni, V. P., Crotts, A. P. S., Lauer, J. T., Richards, G. T., Schneider, D. P., Welty, D. E., Alsayyad, Y., Kumar, A., Lundgren, B., Shanidze, N., Smith, T., Vanlandingham, J., Baugher, B., Hall, P. B., Jenkins, E. B., Menard, B., Rao, S., Tumlinson, J., Turnshek, D., Yip, C.-W., Brinkmann, J., 2006. Average extinction curves and relative abundances for quasi-stellar object absorption-line systems at  $1 < z_{abs} < 2$ . *Mon. Not. R. Astron. Soc.* 367, 945–978.
- Zibetti, S., Ménard, B., Nestor, D. B., Quider, A. M., Rao, S. M., Turnshek, D. A., 2007. Optical Properties and Spatial Distribution of Mg II Absorbers from SDSS Image Stacking. *Astrophys. J.* 658, 161–184.
- Zu, Y., Weinberg, D. H., Davé, R., Fardal, M., Katz, N., Kereš, D., Oppenheimer, B. D., 2011. Intergalactic dust extinction in hydrodynamic cosmological simulations. *Mon. Not. R. Astron. Soc.* 412, 1059–1069.
- Zubko, V., Dwek, E., Arendt, R. G., 2004. Interstellar Dust Models Consistent with Extinction, Emission, and Abundance Constraints. *Astrophys. J. Suppl.* 152, 211–249.
- Zubko, V. G., Mennella, V., Colangeli, L., Bussoletti, E., 1996. Optical constants of cosmic carbon analogue grains - I. Simulation of clustering by a modified continuous distribution of ellipsoids. *Mon. Not. R. Astron. Soc.* 282, 1321–1329.